

# Study on Heat Generation and Distribution in Friction Stir Welding of AA1100 Aluminum Alloy

**H. Aghajani Derazkola\***

Young Researchers and Elite Club, Sari Branch,  
Islamic Azad University, Sari, Iran  
E-mail: h.aghajany31@yahoo.com

\*Corresponding author

**H. Jamshidi Aval**

Department of Mechanical Engineering,  
Babol Noshiravani University of Technology, Iran  
E-mail: h.jamshidi@nit.ac.ir

**Received: 4 November 2014, Revised: 7 January 2015, Accepted: 12 February 2015**

**Abstract:** In this article, the effects of rotational and traverse speeds in friction stir welding (FSW) tool were studied in order to investigate the heat generation and temperature distribution in welding zone of AA1100 aluminium alloy. Computational fluid dynamics method was utilized to simulate the process using commercial CFD Fluent 6.4 package. In order to increase the accuracy of simulation in this study, the welding line which is located between the two workpieces defined with pseudo melt behaviour around the pin tool. Simulation results showed that increasing the rotational speed of FSW tool, leads to an increase in the generated heat and larger stir zone dimension. The obtained result also revealed that the maximum temperature was produced at the advancing side and with increasing tool linear speeds the heat generation experienced growth down trend. With increasing traveling speeds the time to reach maximum temperature in stir zone intensified but the tool rotational speed had no effect on the time to reach to the maximum temperature. More than 85% of the total heat was produced by tool shoulder, and the maximum heat with selected parameters in this study was obtained to be 801°K.

**Keywords:** AA1100 Al Alloy, Computational Fluid Dynamics, Friction Stir Welding

**Reference:** Aghajani Derazkola, H., Jamshidi Aval, H., 'Study on Heat Generation and Distribution in Friction Stir welding of AA1100 Aluminum alloy, Int J of Advanced Design and Manufacturing Technology, Vol. 8/ No. 3, 2015, pp. 9-17.

**Biographical notes:** **H. Aghajani Derazkola** is a PhD Student in Mechanical Engineering at Islamic Azad University of Science and Research branch. **H. Jamshidi Aval** is Associate Professor of Mechanical engineering at the Babol Noshirvani University of Technology, Iran. He received his PhD in Material science and engineering from Sharif University of Technology, Iran. His current research focuses on modelling of dissimilar joints, Microstructure evolution modelling in welding and advanced welding processes.

## 1 INTRODUCTION

Friction stir welding (FSW) is a new process of joining which is considered to have many advantages compared to other welding process, including low cost, high flexibility, lack of pollution, and the need for skilled welders [1]. In this process, the frictional and plastic deformation heat by FSW tools are the key factors that have direct impact on achieving a proper connection [2-4]. On this basis, in order to better understand these factors many researchers worked to simulate this process with computational fluid dynamic (CFD) method. Researchers such as Smith [5] and North [6] were among the first researchers that used the CFD to simulate the FSW process, where they modeled the workpieces as non-Newtonian fluid.

Seidel and Reynolds [7] presented a two-dimensional model to predict material flow in friction stir welding. They observed that at low rotational and linear speed, the composition of the fluids occurs to a large extent horizontally. This effect indicates the need for further analysis of the process three dimensionally. With the development of the 2D material flow, Zhang et al., [8] concluded that the material behind tool had largest deformation compared to other parts around the pin. This angular deformation occurs between 300 to 360 degrees. Material flow during FSW of carbon steel with the use of 3D CFD model was investigated by Nandan et al., [9-10], where they solved the process based on momentum, energy and mass transfer equations. Nandan et. al, defined the non-Newtonian fluid for simulation and predicted the viscosity, strain rate, temperature and stir zone of carbon steel during friction stir welding. Nassar et al., [11] studied on FSW of AZ31B Mg according to Eulerian model and the heat transfer problems. They concluded that by increasing the rotational speed, the weld zone temperature rises and decreases with increasing the linear speed. Ji et al., [12] studied the effect of the FSW tool pin profile on the material flow. The purpose of this article is to investigate the effects of the linear velocity and rotational speed of the tool on the frictional heat generation, temperature distribution and cooling rate of AA1100 aluminum alloy based on the previously developed models. This research was done based on the previous model and their relation to the chemical diffusion equation with plastic deformation of AA1100 aluminum alloy during FSW using a steel tool.

## 2 GOVERNING EQUATIONS

The computational domain in this study, includes the workpiece and the tool inserted inside the workpiece.

The dimensions of the plate and the tool used and the thermo-physical properties of the workpiece and the tool material are given in Table 1. The effects of tool plunge and extraction stages on the total temperature were neglected in this simulation and the temperature and velocity fields were solved assuming steady state behaviour. Three-dimensional plastic flow is represented by the momentum conservation equation in index notation, with  $i$  or  $j = 1, 2$  and  $3$ , representing  $x, y$  and  $z$  directions, respectively [13]:

$$\rho \frac{\partial u_i u_j}{\partial x_i} = -\frac{\partial P}{\partial x_j} + \frac{\partial}{\partial x_i} \left( \mu \frac{\partial u_i}{\partial x_j} + \mu \frac{\partial u_j}{\partial x_i} \right) - \rho U_1 \frac{\partial u_j}{\partial x_1} \quad (1)$$

In Eq. (1),  $u$  is the velocity,  $\rho$  is the density,  $U_1$  is the welding velocity, and  $P$  is the pressure and  $\mu$  is non-Newtonian viscosity that can be determined from flow stress and effective strain rate as follows [14]:

$$\mu = \frac{\sigma_e}{3\dot{\epsilon}} \quad (2)$$

The calculation of viscosity requires local value of strain rate and temperature. In Eq. (2),  $\sigma_e$  indicates the flow stress proposed by Sheppard and Wright [15-16]:

$$\sigma_e = \frac{1}{\alpha} \operatorname{arc} \sinh \left( \frac{Z}{A} \right)^{\frac{1}{n}} \quad (3)$$

Where  $A, a$ , and  $n$  are material constants and  $Z$  is the Zener–Hollomon parameter. The value of constants for AA1100 aluminum alloy are  $A = 5.18 \cdot 10^{10} \text{ S}^{-1}$ ,  $a = 1 \text{ MPa}$ , and  $n = 5.66$  [17]. The Zener–Hollomon parameter,  $Z$ , represents the temperature compensated effective strain rate and is given by [18]:

$$Z = \dot{\epsilon} \exp \left( \frac{Q}{RT} \right) \quad (4)$$

Here  $Q = 158.3 \text{ kJ/mol}$  [19] is the temperature-independent activation energy,  $R$  is the universal gas constant,  $\dot{\epsilon}$  is the effective strain rate and is given by [13]:

$$\dot{\epsilon} = \sqrt{\left( \frac{2}{3} \varepsilon_{ij} \varepsilon_{ij} \right)} \quad (5)$$

Where  $\varepsilon_{ij}$  is the strain rate tensor, defined as [13]:

$$\varepsilon_{ij} = \frac{1}{2} \left( \frac{\partial u_i}{\partial x_j} + \frac{\partial u_j}{\partial x_i} \right) \quad (6)$$

Due to the changes of the physical properties of materials during hot working, having a relation with

mechanical and thermal properties during FSW in simulation procedure is necessary. Based on this factor, the AA1100 aluminum alloy  $C_p$  and  $K$  parameters are defined as [20]:

$$C_p = 929.3 - 0.627T + 1.48 \times 10^{-3}T^2 - 4.33 \times 10^{-8}T^3 \quad (7)$$

$$K = 25.2 + 0.398T + 7.36 \times 10^{-6}T^2 - 2.52 \times 10^{-7}T^3 \quad (8)$$

Similarly for steel tool [21]:

$$C_p = 468.3 - 8.5T + 3.0 \times 10^{-4}T^2 + 1.8 \times 10^{-7}T^3 \quad (9)$$

$$K = 3.8 + 0.092T - 1.8 \times 10^{-4}T^2 + 7.8 \times 10^{-8}T^3 \quad (10)$$

The pressure field was obtained by solving the following continuity equation iteratively with the momentum equations for incompressible single phase flow [9]:

$$\frac{\partial v_i}{\partial x_i} = 0 \quad (11)$$

Where  $v_i$  is the velocity of plastic flow. The steady single phase momentum conservation equations with reference to the co-ordinate system attached to the heat source may be represented as [22]:

$$\rho C_p \frac{\partial(u_i T)}{\partial x_i} = -\rho C_p U_1 \frac{\partial T}{\partial x_i} + \frac{\partial}{\partial x_i} \left( k \frac{\partial T}{\partial x_i} \right) + Q_i + Q_b \quad (12)$$

The heat generated at the interface between vertical and horizontal surfaces of the tool pin and the workpiece may be defined as [22]:

$$Q_i = [(1-\delta)\eta\tau + \delta\mu_f P_N] (\omega r - U_1 \sin\theta) \frac{A_r}{V} \quad (13)$$

Where,  $A_r$  is any small area on the tool pin-work piece interface,  $r$  is the radial distance of the center of the area from the tool axis,  $V$  is the control-volume enclosing the area  $A_r$ ,  $s$  is the maximum shear stress at yielding and  $\theta$  is the angle with the negative x-axis in the counter-clockwise direction,  $\eta$  is the mechanical efficiency (amount of mechanical energy converted to heat energy),  $\delta$  denotes the spatially variable fractional slip between the tool and the workpiece interface,  $\mu_f$  is the spatially variable coefficient of friction,  $\omega$  is the angular velocity, and  $P_N$  is the normal pressure on the surface. An estimate of the viscous dissipation of momentum per unit volume,  $Q_b$ , has been calculated as [23-24]:

$$Q_b = \frac{d\dot{\epsilon}_p}{dV} = \beta\mu\phi \quad (14)$$

Which  $\phi$  is given by [23-24]:

$$\phi = 2 \sum_{i=1}^3 \left( \frac{\partial u_i}{\partial x_i} \right)^2 + \left( \frac{\partial u_1}{\partial x_2} + \frac{\partial u_2}{\partial x_1} \right)^2 + \left( \frac{\partial u_1}{\partial x_3} + \frac{\partial u_3}{\partial x_1} \right)^2 + \left( \frac{\partial u_3}{\partial x_2} + \frac{\partial u_2}{\partial x_3} \right)^2 \quad (15)$$

In Eq. (14),  $\beta$  is an arbitrary constant that indicates the extent of mixing on the atomic scale. The value of  $e$  may tend to 1 for a well-mixed system in molecular scale [25]. The total heat generated at the shoulder/workpiece interface has been partitioned between the work piece and the tool in the ratio given below [22]:

$$q = \frac{(\sqrt{k\rho C_p})_W}{(\sqrt{k\rho C_p})_T} \quad (16)$$

Where the subscripts  $W$  and  $T$  denote the workpiece and the tool, respectively. The analytical expression is based on steady-state one dimensional heat transfer from point heat source located at the interface of dissimilar metals. The heat flux into the work piece is estimated to be 45% of the total heat generated. This relation has been examined experimentally by Lienert et al. [26] and found to be reliable. A heat flux continuity at the shoulder matrix interface yields [22]:

$$k \frac{\partial T}{\partial Z} \Big|_{top} = \frac{J_w}{J_w + J_T} q_1 \quad \text{in the range } R_p \leq r \leq R_s \quad (17)$$

$R_p$  and  $R_s$  represent the tool pin and shoulder radius, respectively and  $q_1$  represents the total rate of heat generation at the shoulder-workpiece interface. It is given by [22]:

$$q_1 = [\eta(1-\delta)\tau + \delta\mu_f P_H] (\omega r - U_1 \sin\theta) \quad (18)$$

At the bottom surface, there is a backing plate and the heat transfer coefficient from the bottom of the workpiece which is not the same as for free convection. The value of the heat transfer at bottom of workpiece was determined by:

$$k \frac{\partial T}{\partial Z} \Big|_{Bottom} = h_b (T - T_a) \quad (19)$$

Where  $h_b$  is the bottom heat transfer coefficient and  $T_a$  is the ambient temperature at 298°K. The heat transfer coefficient at the bottom face depends on the local temperature and is given by the following relation [27]:

$$h_b = h_{b0} (T - T_a)^{0.25} \quad (20)$$

Where  $h_{bo}$  is the heat transfer parameter for the bottom surface. As Eq. (20), shows this parameter is constant and it has a different unit than the heat transfer coefficient which is spatially variable. At the top surface, heat transfer is due to both convection and radiation and is given by:

$$-k \frac{\partial T}{\partial Z} \Big|_{top} = B\epsilon(T^4 - T_a^4) + h_t(T - T_a) \quad (21)$$

B is the Stefan–Boltzmann constant ( $5.67 \times 10^{-16} \text{ J.K}^{-4}.\text{m}^{-2}.\text{s}^{-1}$ ),  $\epsilon$  is the emissivity and  $h_t$  is the convective heat transfer coefficient at the top surface. The computed temperature values were found to be insensitive to the values of  $h_t$  and its value was taken as zero for simplicity. During the simulation, linear and rotational speed of the tool pin and shoulder were performed separately. For this purpose, the sum of the rotational and linear speeds were defined as separate components in a Cartesian coordinate system. Fig. 1 shows the detachment of linear and rotational speeds into a unified coordinate system.

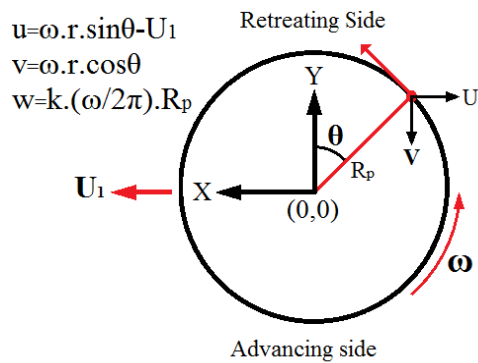


Fig. 1 Detachment of linear and rotational speeds

Velocities at the tool pin periphery have been defined in terms of tool translation velocity and the tool pin angular velocity [28]:

$$u = (\omega R_p \sin\theta - U_1) \quad (22)$$

$$v = (\omega R_p \cos\theta) \quad (23)$$

$$w = k \left( \frac{\omega}{2\pi} \right) R_p \quad (24)$$

Where K represents the thread angle on the tool pin. Similarly, at the shoulder–work piece interface, the velocity boundary conditions may be written as [28]:

$$u = (\omega r \sin\theta) \quad (25)$$

$$v = (\omega r \cos\theta) \quad (26)$$

At all other surfaces, temperatures are set to ambient temperature (298K).

### 3 PROCESS MODELING AND MESH GENERATION

According to the FSW pattern, the tool passed three main steps from start to the end of welding process. The first step is called plunging which means that the tool penetrates into the joint line. The second step is mixing of the joint line and the last step is the tool exit after complete welding. In this study, the first and last phases of tool situation have been neglected and the simulation proceeds on the tool situation during moving forward. In this model a frustum pin with  $2^\circ$  tilt angel was designed as FSW tool with 10 mm shoulder diameter. The pin big diameter of pin was 6mm, the small diameter was 4mm and the pin height was 2.8 mm. The base metal assumed as non-Newtonian fluid with visco-plastic behaviour and density was based on AA1100 aluminium alloy.

The Tetrahedral/Hybrid elements with T-grid combination shape were used for the mesh generation of tool and workpiece. The region close to the pin tool and the tool itself required a much finer mesh to evaluate the heat transfer model and viscous flow. A sizing function on the tool and workpiece was used to generate different volume sizes. The sizing function uses a start size, growth rate and maximum size. For the fine mesh pictured in Fig. 2, a start size was 0.1 mm, growth rate 1.3 mm, and a maximum size of 1.5 mm. For this meshing scheme, the total number of volumes for the lateral case was 3,864,200 volumes.

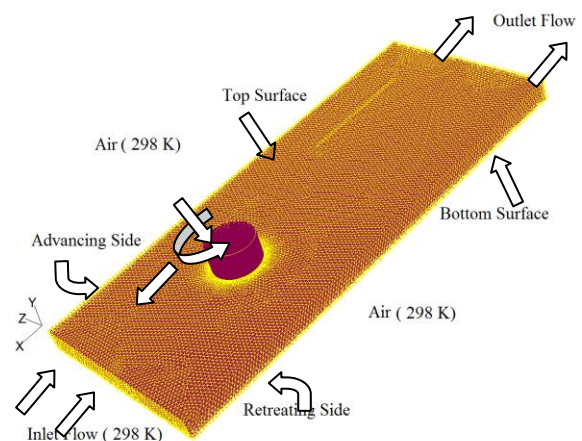


Fig. 2 Meshed model of the FSW process

The cross section of the model with meshes and used parameters are shown in Fig. 3, and Table 1, respectively.

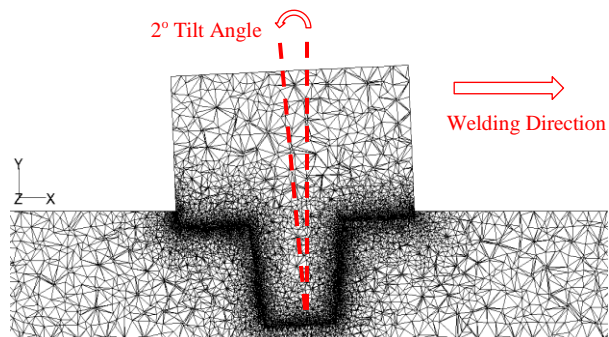


Fig. 3 Meshed model of the tool

Table 1 Tool Parameters

Tool Parameters	Value
$\omega$ , rpm	500, 630, 710, 800
V, mm/min	25, 40, 63, 80
Workpiece Melting Point, °C	690
Workpiece density (Kg.m <sup>-3</sup> )	2710
Workpiece Length (mm)	200
Workpiece width (mm)	100
Workpiece thickness (mm)	3
Tool shoulder radius	10
Pin big radius	3
Pin small radius	2
Pin height	2.8
Tool tilt angle	2
Tool Material	HSS Steel
Tool density (Kg.m <sup>-3</sup> )	7821
$\delta_0$	2.3
$\eta$	0.004
$\mu_0$	0.41
$\epsilon$	0.5
$P_N$ , N	10e8

## 4 RESULTS AND DISCUSSION

### 4.1. Heat generation rate

Heat generated during FSW process is dependent on many mechanical parameters. In this study, the term heat production rate, is the ratio of total heat generated by each part of the tool in different rotational speed, linear velocity, tool offset and tool tilt angle. With the assumptions mentioned in the previous section it can be concluded that the study of the rate of heat production in each part of the tool depends on the extent of the contact area with the workpiece.

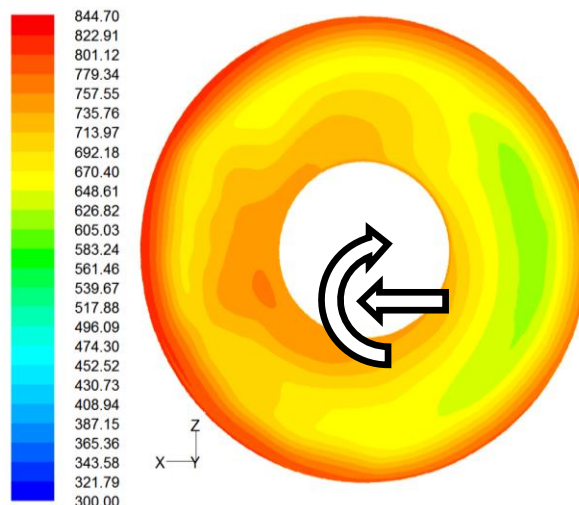


Fig. 4 Heat generated by the tool shoulder (The numbers are based Kelvin degrees)

Figure 4 shows the heat generated by the shoulder at 800 rpm rotational speed and linear speed of 25 mm/min after 13 seconds. As seen in the figure, the maximum amount of heat generated in the exterior portion of the shoulder is 801.12°K. The amount of heat is equal to 83% of the melting temperature of the aluminium base metal. The tool tilt angle causes the amount of heat generated in front of the tool shoulder become more than the tool behind. Figure 5 shows the heat produced by the tool pin body after 13 seconds from the start of welding. The results show that the heat generated by the tool pin is less than the amount of heat generated by the tool shoulder.

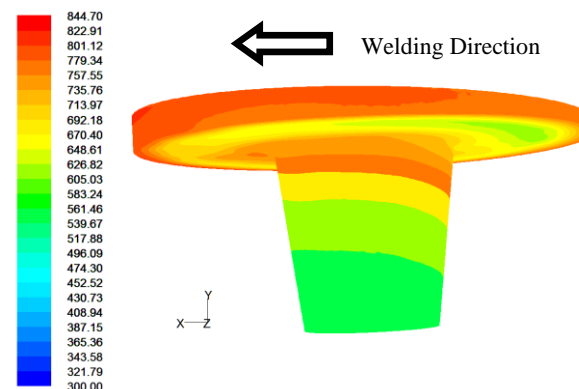


Fig. 5 Heat generated by the pin (The numbers are based on degrees Kelvin)

The amount of heat generated by the tool pin area increases the temperature to approximately 387°K which is close to 12% the melting temperature of the base metal. The results of the pin tool investigation showed that the lowest heat is generated at the bottom of the pin near the bottom of the workpiece. The cause of this phenomenon is related to the distance of the pin tool

beneath from the main heat source (tool shoulder) and small contact area with the workpiece, where the temperature gets to 387°K in this region. In general it can be concluded that the maximum heat generated in this process is created by the tool shoulder and it is due to the greater contact area between this part of the tool relative to other parts with the workpieces.

The maximum heat generated by the shoulder and the pin in different rotational and traverse speeds are shown in Fig. 6. As seen in Fig. 6, with increasing rotational speed more frictional heat is generated and with increasing tool traverse speeds, the amount of generated heat decreases in each of the tool components. In this study, the maximum heat generated was achieved at the 800 rpm rotational speed and 25 mm/min linear velocity and the lowest heat was generated at 500 rpm rotational speed and 80 mm/min linear velocity, respectively. Based on the results, the maximum generated heat with tool shoulder is almost five times the pin tool.

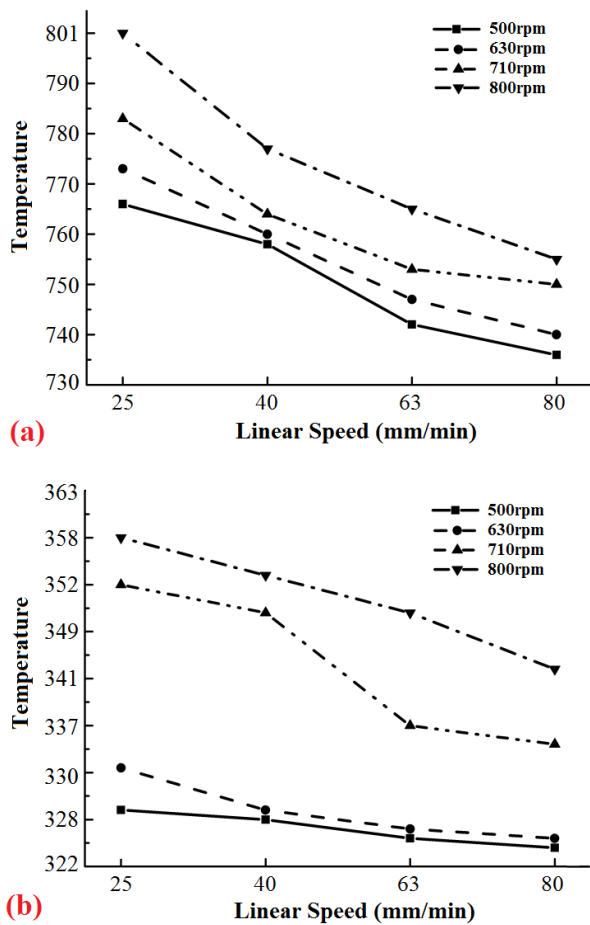


Fig. 6 Heat generated by (a) shoulder and (b) pin (Kelvin) in different rotational and linear speeds

4.2. Heat generation in stir zone

Figure 7 shows the results of generated heat with tool from the start process until heat up to maximum temperature. The maximum heat was generated after 20 seconds at 800rpm rotational speed and 25 mm/min traverse speed. Because the chosen tool direction was CCW, the temperature diffusion on the advancing side was more than retreating side. The results showed that the temperature distribution along the heat generated zone by the tool shoulder, starts from the upper area of the joint.

As mentioned in the previous section, owing to more heat generated by the tool shoulder relative to other parts of the tool, heat penetration towards the interior region of the workpiece takes place from upper area of the workpiece. After a few seconds, along the rotating tool, the heat diffuse into the workpiece and the ambient temperature around the tool rises and causes heat flow penetrate into the lower regions of the workpiece. Due to the lower heat produced by the tool pin bottom, heat penetration to the workpiece end zone took place with some delay.

After the temperature distribution, the heat reaches the tool bottom and the low heat produced by tool pin beneath added to the bottom of the workpiece. This causes more heat distribution in the workpiece lower part. On the other hand, it is possible to observe that the heat inside the workpiece expands inward from above the progressive region.

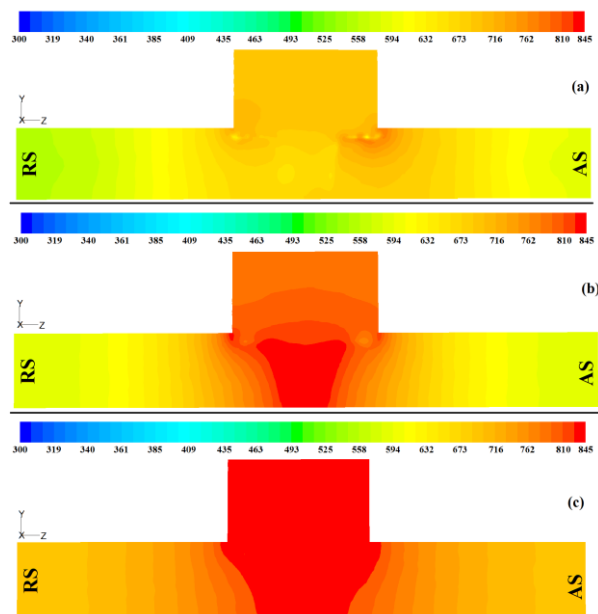


Fig. 7 Welding heat generated by the tool after (a) 5s, (b) 10s and (c) 20s (the results are based on °K)

4.3. Heat distribution

Figure 8 shows the heat distribution produced by 800 rpm rotational speed and 25 mm/min linear velocity on the surface of the workpiece from 5s after start welding till 20s thereafter. As can be seen the heat distribution in the advancing side is more than retreating side. The tool rotation direction leads the heat to advancing side. This phenomenon is the consequence of material flow that increases during stirring. The maximum temperature of about 801°K generated under the tool shoulder. The presence of high temperature in the surrounding area of the tool was caused by the heat generated from the high strain rate close to the tool. The high temperature contours were nearly circular due to the low welding speed of 25 mm/min, but the temperature distribution was not symmetric about the tool axis. The temperature gradient was much steeper in front of the tool than behind the tool. The material before welding was about 298°K, and the temperature behind the tool was over 385°K in the end of the workpiece after 20s from start welding.

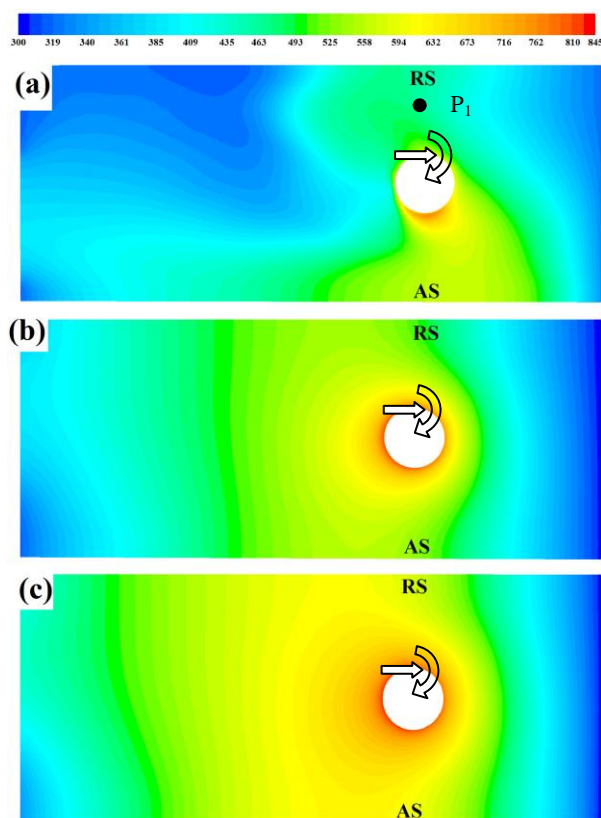


Fig. 8 Heat distribution at top surface of workpiece after (a) 5s, (b) 10s and (c) 20s (the results are based on °K)

As seen in Fig. 8, at the beginning of the process the heat diffusion is not so visible at retreating side. With increasing tool rotation, the heat generated in the retreating side grows up and on the other hand the advancing side temperature is convected to the

retreating side. Finally after 20 seconds, the thermal conditions were reached to the steady state.

4.4. Effects of tool rotational and traverse speeds

Mechanical parameters of FSW have effects on the heat generated during welding. These parameters have direct effect on the time to reach maximum temperature, heat distribution and cooling rate. The results of the simulation are shown in Fig. 9. According to the defined FSW process parameters in this study, the maximum temperatures generated in 500, 630, 710 and 800 rpm rotational speeds and 25, 40, 63 and 83 mm/min linear velocities were calculated, respectively. With speedup of the tool rotational speed, the generated frictional heat increases. On the other hand, with an increase in traverse speed the lasting heat source in stir zone is reduced, causing a rapid loss of heat, which thereby decreasing the heat generated. Due to the selected parameters in this study, the maximum heat was produced at 800 rpm rotational speed and 25 mm/min linear velocities. The amount of heat generated in this welding parameter setting was 845°K. By reducing the rotational speed during the linear speed of 25 mm/min, the maximum temperature from 845°K at 800 rpm rotational speed descend to 786°K at 500 rpm. By increasing the linear speed velocity from 25 mm/min to 80 mm/min, the produced temperature at 800 rpm rotational speed drops from 801°K down to 771°K.

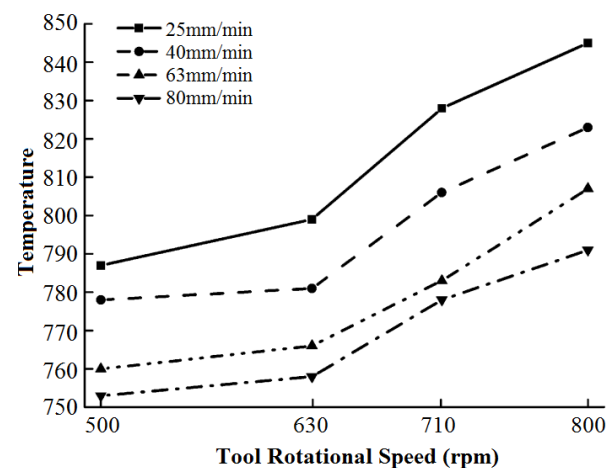
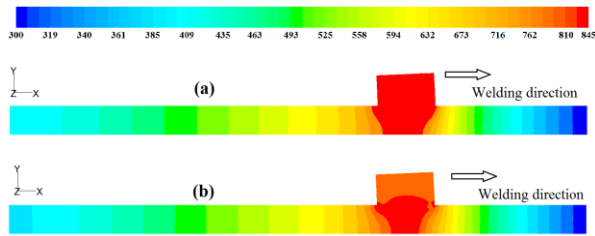


Fig. 9 Total heat generation at different rotational and linear speeds

The main effect of linear velocity during FSW process is durability of heat source in stir zone. At low rotational speed, the heat source endurance inside the tool is prolonged, hence the tool loses less heat, and the plastic zone dimension would be larger. Figure 10, shows longitudinal section of these effects at 800 rpm tool rotational speed with 25mm/min and 80 mm/min traveling speeds.



**Fig. 10** Total heat generation at different rotational and linear speeds

This decreasing trend occurs similarly in other rotational speeds. Furthermore, in addition to the direct effect on the heat amount, linear and rotational velocities are also effective on the time duration to reach to the maximum temperature.

For example, the effect of linear velocity on producing the frictional heat at the  $P_1$  at the 800 rpm rotational speed is shown in Fig. 11. As can be seen, by increasing the linear velocity from 25 mm/min to 80 mm/min, the time to reach the maximum temperature generated during the process was decreased. This phenomenon is caused by additional pressure and torque, by faster forward moving and increased heat production of plastic deformation in the tool pin beneath.

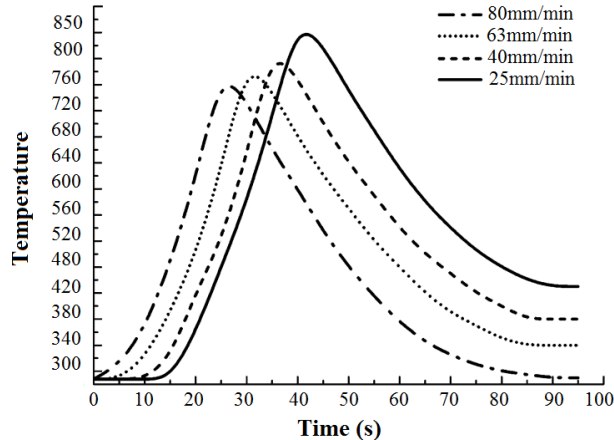


**Fig. 11** Effect of linear velocity on the time to reach maximum heat (the results are based on °K)

The results show that the maximum temperature was produced 27 seconds after starting transverse moving at 80mm/min linear velocity. This issue implies that the maximum frictional heat is created after 36mm forward moving. The time to reach the maximum temperature in 25, 40 and 63 mm/min were 42, 37 and 32 second respectively. These numbers show that the maximum frictional heats at the listed linear velocity are obtained after 17.5, 24.6 and 33.6 mm moving forward. As

mentioned earlier, by increasing the tool rotational speed the maximum produced temperature increases.

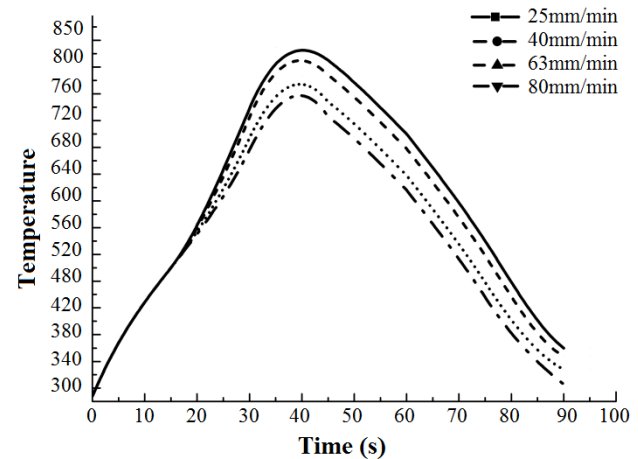


**Fig. 12** Effect of rotational velocity for time to reach maximum heat (the results are based on °K)

Figure 12 shows the effect of tool rotational speed for time to reach maximum heat generated the  $P_1$  in 25 mm/min linear velocity. As seen in Fig. 12, the tool rotational speed variations have no severe effects on the time to reach to the maximum temperature.

## 5 CONCLUSION

In this study, friction stir welding of aluminium AA1100 was simulated 3D, using computational fluid dynamics. The temperature variations were assessed at different rotational and linear velocities. The simulation results are as follows:

1. Investigation on various parts of the tool revealed that the maximum heat is generated by the tool shoulder; this is due to larger tool shoulder surface contact with the workpiece.
2. The results show that 80 to 85 percent of the total heat is generated by the tool shoulder in FSW AA1100 aluminium alloy.
3. Based on the selected parameters in this study, during FSW of AA1100 aluminium alloy the highest temperature was produced at 800 rpm (845°K), and the lowest temperature was produced at 500 rpm rotational speed and 80 mm/min linear velocity (752°K).
4. The heat distribution start from contact area between workpiece and tool shoulder and the temperature diffusion on the advancing side was more than the retreating side.

5. With increasing the linear velocity, the time to reach the maximum temperature generated during the process was decreased. On the other hand the tool rotational speed variations have no severe affects on the time to reach to the maximum temperature.

---

## REFERENCES

---

- [1] Patil, H. S., Soman, S. N., "Influence of Weld Process Parameters on Material Characterization of Friction Stir Welded Joints of Aluminium Alloy AA6061-T6", *International Journal of Advanced Design and Manufacturing Technology*, Vol. 6, No. 4, 2013, pp. 9-15.
- [2] Santiago, D., Urquiza, S., Lombera, G., and Vedia, L., "3D Modeling of Material Flow and Temperature in Friction Stir Welding", *Soldagem & Inspeção*, Vol. 14, No. 3, 2009, pp. 248-256.
- [3] Hamilton, R., MacKenzie, D., and Li, H., "Multi-physics simulation of friction stir welding process", *Engineering Computations: International Journal for Computer - Aided Engineering and Software*, Vol. 27, No. 8, 2010, pp. 967-985.
- [4] Zhang, Z., Zhang, H. W., "A fully coupled thermo-mechanical model of friction stir welding", *International Journal of Advanced Manufacturing Technology*, Vol. 37, 2008, pp. 279-293.
- [5] Smith, C., Bendzsak, G., North, T., Hinrichs, J., Noruk, J., and Heideman, R., "Heat and Material Flow Modeling of the Friction Stir Welding Process", 11<sup>th</sup> International Conference on Computer Technology in Welding, Detroit, United State, 1999.
- [6] North, T., Bendzsak, G., and Smith, C., "Material Properties Relevant to 3-D Modeling", 2<sup>nd</sup> International Friction Stir Welding Symposium, Gothenburg, Sweden, 2000.
- [7] Seidel, T. U., Reynolds, A. P., "Two-dimensional friction stir welding process model based on fluid mechanics", *Science and Technology of Welding and Joining*, Vol. 8, 2003, pp. 175-183.
- [8] Zhang, W., DebRoy, T., Palmer, T. A., and Elmer, J. W., "Modeling of ferrite formation in a duplex stainless steel weld considering non-uniform starting microstructure", *Acta Materialia*, Vol. 53, No. 16, 2005, pp. 4441-4453.
- [9] Nandan, R., Roy, G., and DebRoy, T., "Numerical simulation of three dimensional heat transfer and plastic flow during friction stir welding", *Metallurgical and Materials Transactions A*, Vol. 37, No. 4, 2006, pp. 1247-1259.
- [10] Nandan, R., Roy, G., Lienert, T., and DebRoy, T., "Numerical modelling of 3D plastic flow and heat transfer during friction stir welding of stainless steel", *Science and Technology of Welding and Joining*, Vol. 11, No. 5, 2006, pp. 526-537.
- [11] Nassar, H. W., Khraisheh, M. K., "Simulation of Material Flow and Heat Evolution in Friction Stir Processing Incorporating Melting", *Journal of Engineering Materials and Technology*, Vol. 134, 2012, pp. 61-67.
- [12] Ji, S. D., Shi, Q. Y., Zhang, L. G., Zou, A. L., Gao, S. S., and Zan, L. V., "Numerical simulation of material flow behavior of friction stir welding influenced by rotational tool geometry", *Computational Materials Science*, Vol. 63, 2012, pp. 218-226.
- [13] Arora, A., Zhang, Z., Deb, A., and DebRoy, T., "Strains and strain rates during friction stir welding", *Scripta Materialia*, Vol. 61, 2009, pp. 863-866.
- [14] Zienkiewicz, O. C., Corneau, I. C., "Visco-Plasticity Solution by Finite-Element Process", *Archives of Mechanics*, Vol. 24, 1972, pp. 872-889.
- [15] Sheppard, T., Wright, D. S., "Determination of Flow-Stress .1. Constitutive Equation for Aluminum Alloys at Elevated-Temperatures", *Metals Technology*, Vol. 6, 1979, pp. 215-223.
- [16] Sheppard, T., Wright, D. S., "Determination of Flow-Stress .2. Radial and Axial Temperature Distribution during Torsion Testing", *Metals Technology*, Vol. 6, 1979, pp. 224-229.
- [17] Sheppard, T., Jackson, A., "Constitutive equations for use in prediction of flow stress during extrusion of aluminium alloys", *Materials Science and Technology*, Vol. 13, 1997, pp. 203-209.
- [18] Zener, C., Hollomon, J. H., "Effect of Strain Rate upon Plastic Flow of Steel", *Journal of Applied Physics*, Vol. 15, 1944, pp. 22-32.
- [19] Sheppard, T., Wright, D. S., "Determination of flow stress: Part 1 constitutive equation for aluminium alloys at elevated temperatures", *Metals Technology*, Vol. 6, 1979, pp. 215-223.
- [20] Davis, J. R., "Nonferrous Alloys and Special-Purpose Material", *ASM Handbook*, Vol. 2, Ohio, 1990.
- [21] Brandes, E. A., Brool, G. B., "Smithells Metals Reference Book", 8th Ed, Elsevier, Oxford, 2004.
- [22] Nandan, R., Roy, G., Lienert, T. J., and Debroy, T., "Three-dimensional heat and material flow during friction stir welding of mild steel", *Acta Materialia*, Vol. 55, 2007, pp. 883-895.
- [23] Carslaw, H. S., Jaeger, J. C., "Conduction of heat in solids", 2<sup>nd</sup> Ed, Oxford, Clarendon Press, 1959, pp. 87-89.
- [24] Ayer, R., Jin, H. W., Mueller, R. R., Ling, S. and Ford, S. "Interface structure in a Fe-Ni friction stir welded joint", *Scripta Materialia*, Vol. 53, 2005, pp. 1383-1387.
- [25] Nandan, R., Prabu, B., De, A., and Debroy, T., "Improving Reliability of Heat Transfer and Materials Flow Calculations during Friction Stir Welding of Dissimilar Aluminum Alloys", *Welding Journal*, Vol. 86, 2007, pp. 313-322.
- [26] Lienert, T. J., Stellwag, W. L., Grimmert, B. B., and Warke R. W., "Friction Stir Welding Studies on Mild Steel", *Welding Journal*, Vol. 82, 2003, pp. 1s-9s.
- [27] Schuhmann, R., "Metallurgical Engineering", Vol. 1: Engineering Principles, Cambridge press, Addison-Wesley Press, 1952.
- [28] Liechty, B. C., Webb, B. W., "Modeling the frictional boundary condition in friction stir welding", *International Journal of Machine Tools and Manufacture*, Vol. 48, 2008, pp. 1474-1485.